CHAPTER 5

Nano-cryospray: Thermal effect of adjuvants on cryoablation

The present study proposes novel method to make cryospray a preferred method in the treatment of larger lesions. The lower thermal conductivity of tissue reduces the rate of energy transfer inside it, which results in a longer duration of treatment and causes discomfort to the patient. Researchers working in the field of cryosurgery [51, 132, 180, 187] have improved the rate of energy transfer inside the tissue through the administration of adjuvant in the lesion. Cryosugery and cryospray are the branches of cryotherapy: cryosurgery is used to treat lesion occurring inside the body whereas cryospray is used for cutaneous lesions. In the current scenario, administration of nanoparticles inside the tissue for cryosurgery is well explored by the researchers. They can be injected directly as nanofluid in the biological matrix of the tissue. However, similar approach could not be opted for cryospray because it deals with the superficial lesions. The adjuvant administration in superficial lesion requires drug administration through trnasdermal route which was a challenging task in past decade. Because the stratum corneum (the outermost layer of skin) constrains the transport of external agents through the transdermal route; however it also saves our body from pathogens. Specially formulated drugs in terms of size, surface charge and composition were necessary to meet the requirement of transdermal transport. Therefore, in the past decade, there were two prerequisites of transdermal transport of drugs: (i) Methods to circumvent stratum corneum and (ii) Formulation of drugs. Due to this reason adjuvant assisted cryospray is less explored in the literature.

However, at present, there are four physical enhancement methods to evade the stratum corneum [162]. They are microneedles, inophorosis, sonophorosis and velocity based devices. Very recently, heat based removal of stratum corneum has replaced the traditional process like tapes stripping, mechanical abrasion and chemical treatment. Since its inception from the first generation three-day patch, that delivers scopolamine to treat motion sickness, to the third generation delivery systems like microneedles, microdermabrasion etc., transdermal drug delivery has revolutionised the medical practice [125]. Apart from that, innovations in the field of nanotechnology has provided leverage to researchers in the synthesis of nano-meter sized specially formulated drugs for various biomedical applications [116]. Literature suggests that the pronounced effect of nanoparticles (as adjuvants) can be easily acknowledged in the field of molecular diagnostic, cancer therapy, gene delivery vehicles and antibacterial drug [118, 128]. Nanoparticle assisted drug delivery has also gained immense popularity in dermatology such as photoprotection, barrier creams, treatments of hair disorders.

Thus, acknowledging the advancement in transdermal drug delivery systems which leads to promising results of nanoparticle administration through stratum corneum [53, 163], the motive of the research is to explore an adjuvant assisted approach to increase the efficacy of cryospray. The reason behind the administration of adjuvant in the lesion is to improve the thermophysical properties of the lesion which will increase the rate of heat transfer in the lesion and decrease the duration of treatment. Moreover, larger lesions can also be treated through the proposed approach. It has been observed in the previous study (chapter 3) that device modifications can eliminate the existing limitation of cryospray process [155, 156]. Hence, customised multihole nozzles (MHN) are also used to spray the cryogen on adjuvant loaded phantom in the present study.

5.1 Materials and Method

All the three nanoparticles (MgO, Al_2O_3 and Fe_3O_4) used in the preparation of nano-phantom are procured from Adnano Technologies. Here, nano-phantom means phantom loaded with nanoparticles and normal-phantom means phantom without nanoparticles. The equipment used in the preparation of nanofluids are Magnetic stirrer (Contech) and ultrasonicator (labmann). Span 20 surfactant is used to increase the stability of nanofluid. The other materials and devices used in the preparation of phantom and characterisation of results respectively are kept same as in Chapter 3.

A layered phantom approach is used to make nano-phantom (shown in fig. 5.1). It has been observed that wherever nanoparticles are administered inside the body through

(a) MgO nano-phantom (b) Al_2O_3 nano-phantom

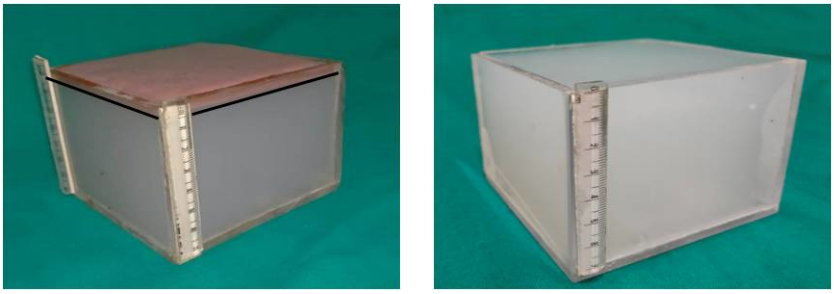

(c) Fe_3O_4 nano-phantom (d) Normal-phantom

Figure 5.1: Phantom used in the study

transdermal route they accumulate in the vicinity of administration. Their diffusion depends on the amount and duration of the dosing [161, 165]. So, two layers are made in the nano-phantom: the upper layer consists of agarose gel loaded with the adjuvant (nanoparticles) and the lower layer is made up of agarose gel only. The concentration of adjuvant is taken as 0.2% w/v. A 200 ml volume of double distilled water is used as the base fluid in the synthesis of nanofluid. The base fluid and adjuvant are stirred in the magnetic stirrer for 45 minutes in the presence of 5% w/v surfactant (Span 20). The prepared mixture is further sonicated in a sonicator at 20 KHz for another 60 minutes. In order to make the gel, agarose (0.6 w/v) is added in the prepared mixture afterward and heated for 3 minutes at 900 W in a microwave oven. The solution is then allowed to solidify over the lower agarose gel at room temperature for 8 hours. Thickness of upper layer is taken as 5 mm to mimic the thickness of the dermis [142]. The lower layer of agarose is made using the procedure followed in Chapter 3. The quantity of ingredients and procedure followed in the preparation of nano-phantom is kept same for all the three nano-particles.

5.2 Characterisation of nanofluid

Skin is one of the largest parts of the body in terms of surface area and weight. It serves various functions of the body like thermoregulation, protecting body from foreign pathogen

etcetra. So, its thickness and porosity depends on the orientation and age of the person. Several authors have analysed the role of nanoparticle's size on the skin absorbance [114]. It has been reported that nanoparticles less than 50 nm in size can penetrate easily in the human skin [32, 58]. The TEM and SEM images of nanoparticles are shown in fig. 5.2, fig. 5.3 and fig. 5.4. It can be seen in the TEM images that the particle size of all the nanoparticles are less than 50 nm, hence their penetration can be ensured. Moreover, it can be observed through the SEM images that MgO and Fe_3O_4 nanoparticles are spherical in shape whereas Al_2O_3 nanoparticles possess non-spherical rod like structures. It should be noted here that the administration of nanoparticle depends on several other factors like surface chemistry, porosity of skin, dose and exposure as well. The study of those parameters are beyond the scope of the present work. Hence, two most important parameters, i.e. shape and size of nanoparticles are discussed here. The XRD pattern of the different nanoparticles used in the study are shown in fig. 5.5. The peaks obtained at various 2θ values and its corresponding planes ensure the purity of the nanoparticles used in the study. The crystallographic parameters confirm the formation of cubic, orthorombhic and rhombohedral crystal in MgO, Al_2O_3 and Fe_3O_4 nanoparticles respectively. The observed patterns are similar to the previously reported results [12, 112, 147]. In order to verify the stability of the nanofluid, the concept of isoelectric point (IEP) is employed in the analysis of stability of nanofluid. At IEP, the zeta potential of solid is zero [89]. This indicates less electrostatic force of repulsion and the nanoparticles will agglomerate due to the Vanderwall force of attraction [140]. If the pH is far away from the IEP then stability of nanofluid can be ensured due to the large repulsion force between the nanoparticles. The pH of nanofluid is measured with the digital pH meter. The pH of prepared MgO, $Al_2O_3$and Fe_3O_4 nanofluids are found to be 8.5, 8 and 7.5 respectively. However, the IEPs of MgO, $Al_2O_3$and Fe_3O_4 nanoparticles are 10.5, 9.1 and 8.4 respectively [95, 103], which means the nanofluids are stable.

Nanoparticles are used to enhance the thermophysical properties of the nano-phantom. They possess excellent thermal conductivity and the aim to introduce nanoparticles as adjuvant is to increase the same in nano-phantom. The thermal conductivity of different nano-phantoms are determined experimentally through Hot Disk TPS 500 thermal constant analyser at 27 ^{0}C. Thermal conductivity of nano-phantoms are estimated to be 0.71±0.01 W/mK, 0.67±0.01 W/mK and 0.63±0.01 W/mK for MgO, Al_2O_3 and Fe_3O_4 respectively. The conductivity of normal-phantom is estimated as 0.59±0.02 W/mK.

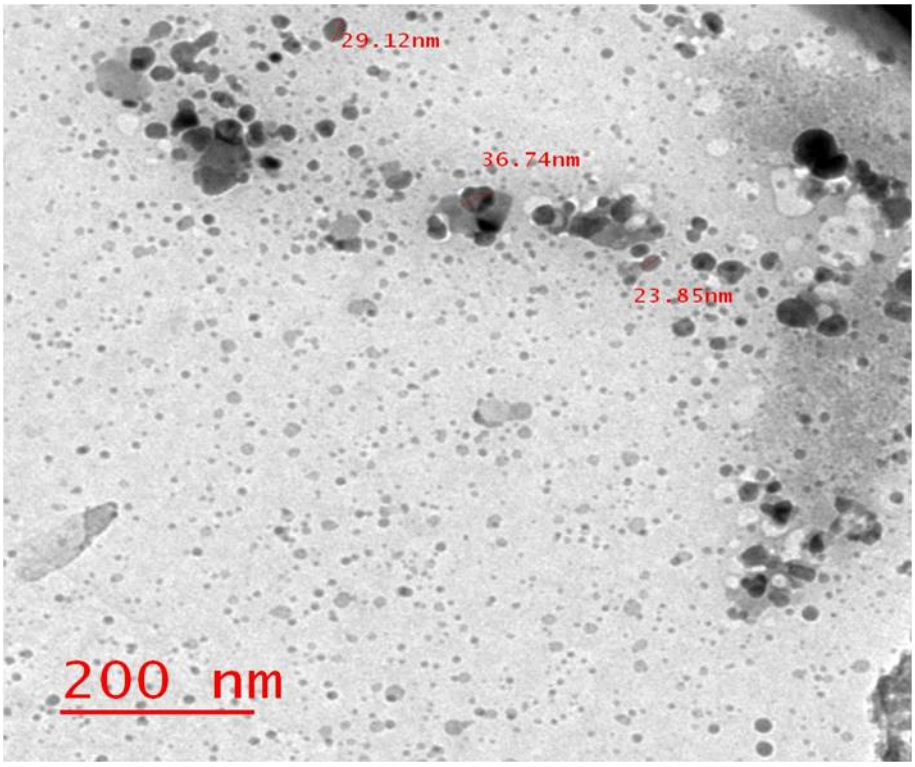

(a) TEM images of MgO nanoparticles

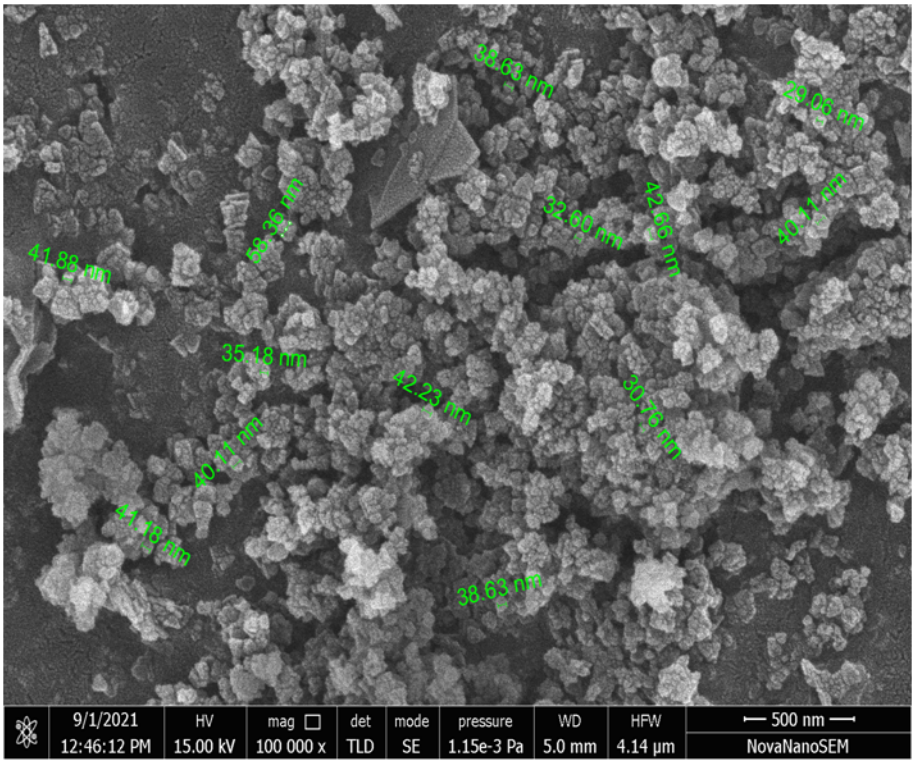

(b) SEM images of MgO nanoparticles

Figure 5.2: Charactersation of MgO nanoparticles

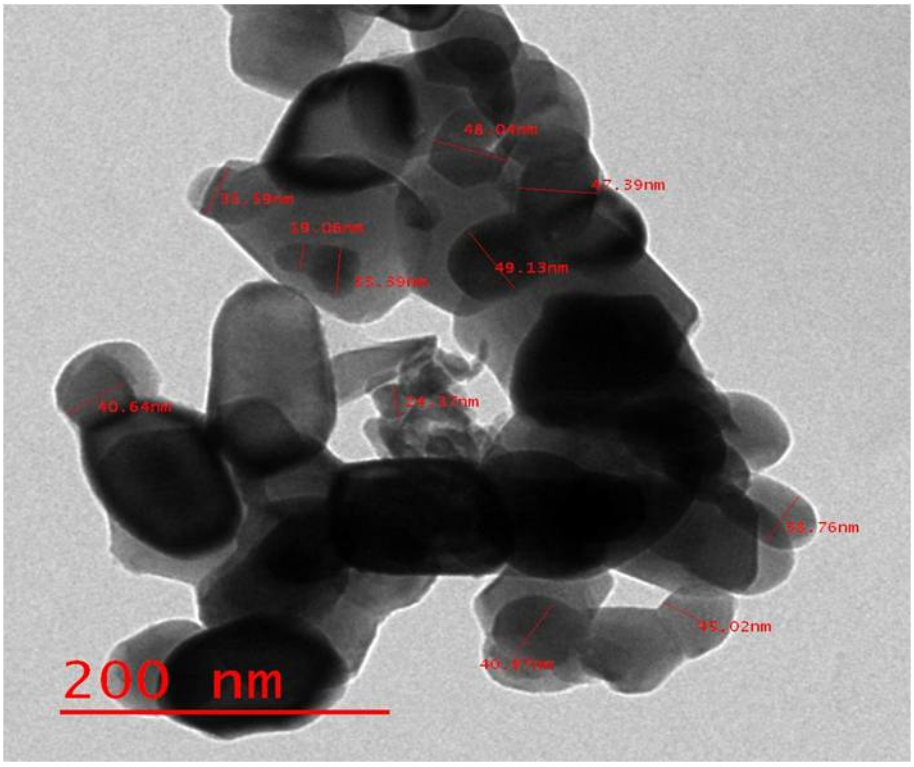

(a) TEM images of Al_2O_3 nanoparticles

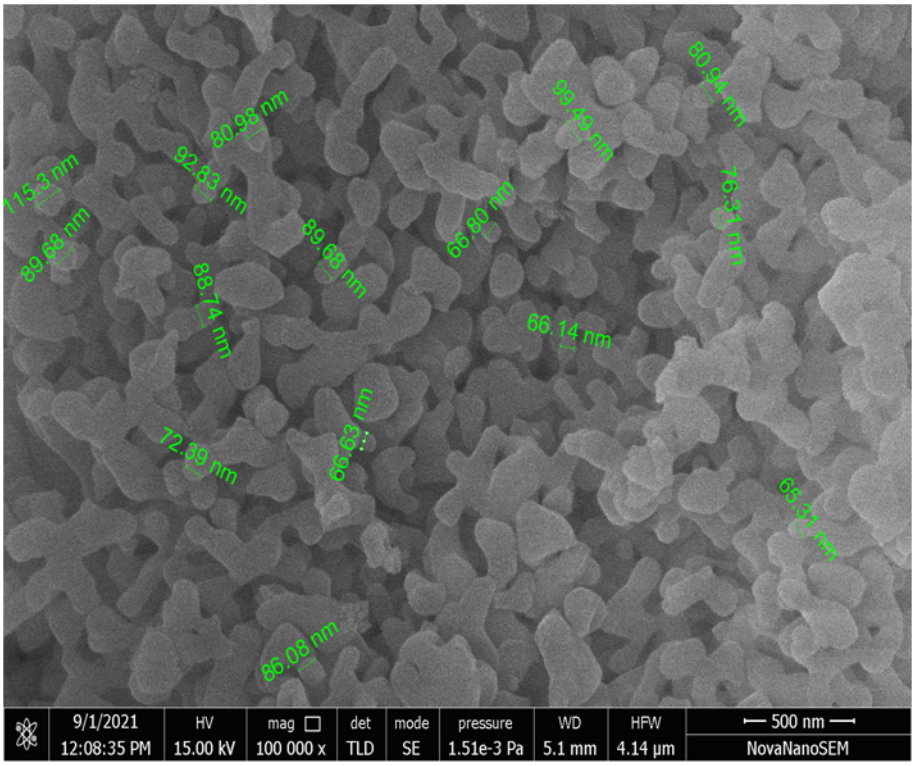

(b) SEM images of Al_2O_3 nanoparticles

Figure 5.3: Characterisation of Al_2O_3 nanoparticles

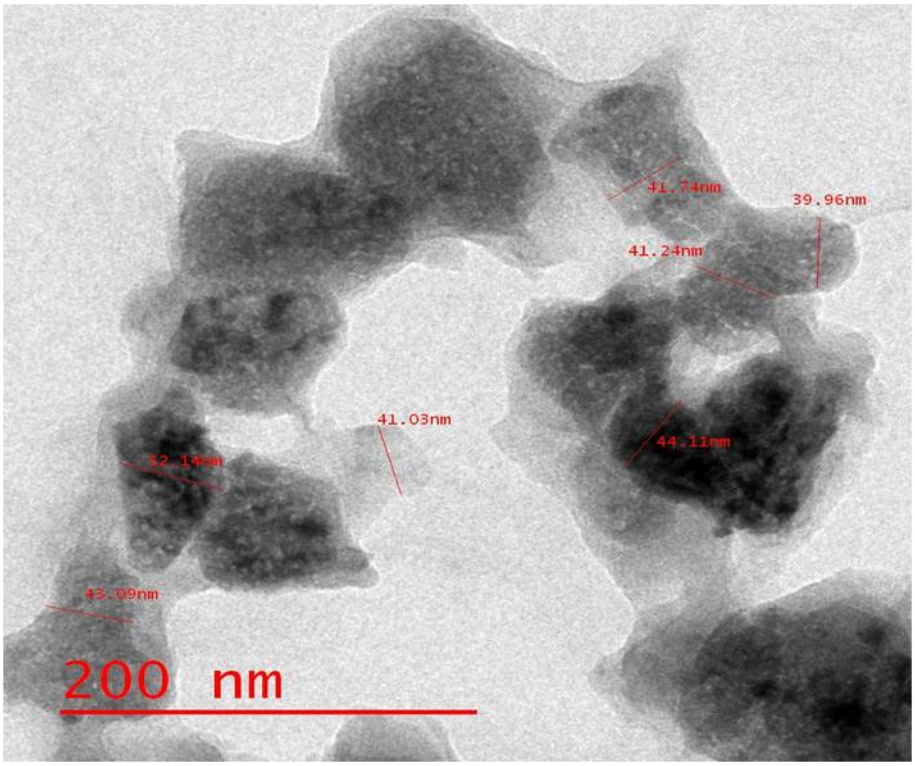

(a) TEM images of Fe_3O_4 nanoparticles

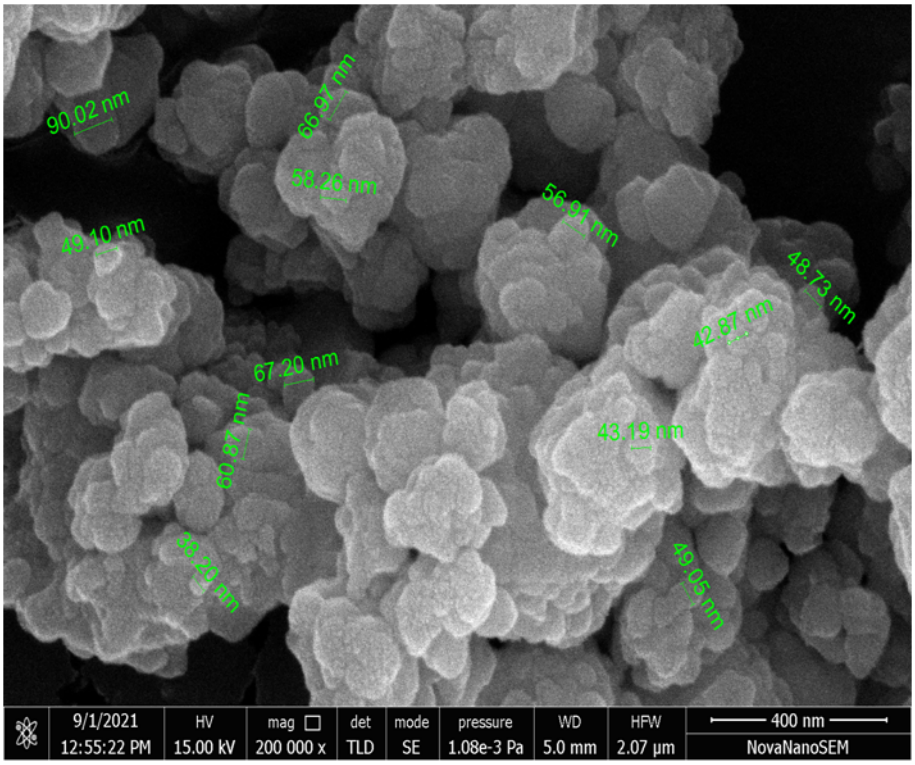

(b) SEM images of Fe_3O_4 nanoparticles

Figure 5.4: Charactersation of Fe_3O_4 nanoparticles

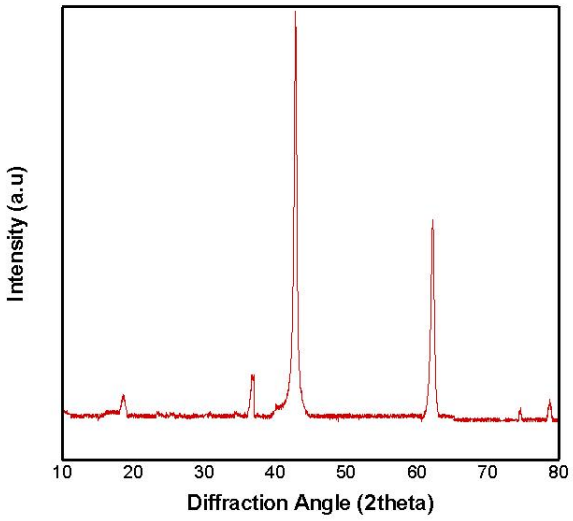

(a) XRD Pattern of MgO nanoparticles

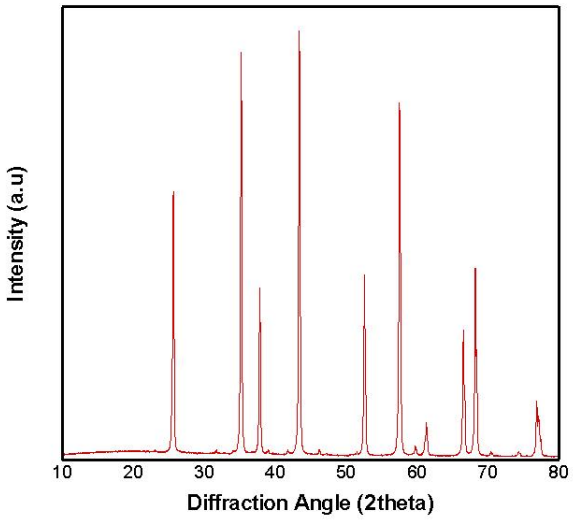

(b) XRD Pattern of Al_2O_3 nanoparticles

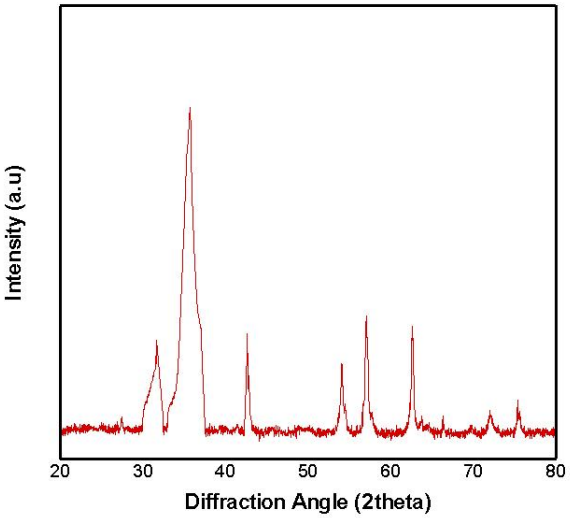

(c) XRD Pattern of Fe_3O_4 nanoparticles

Figure 5.5: XRD Pattern of nanoparticles

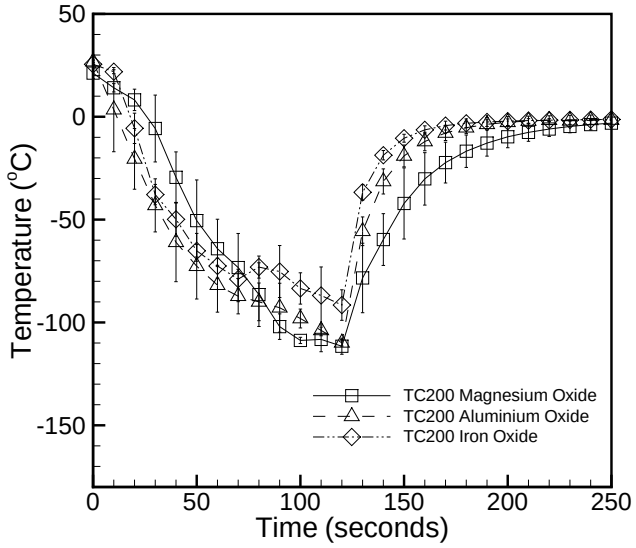

Figure 5.6: Transient temperature curves of thermocouples placed at 2 mm below the gel surface and 0 mm away (TC200 location) from CS with 95% confidence interval for different nano-phantoms

5.3 Uncertainty Analysis

Reproducibility of results is an important aspect of any experimental analysis. It is expected that experiments with identical boundary and initial conditions should produce same result. The deviation in the results of similar experiment is termed as uncertainty in the measurement. There can be several factors influencing uncertainty in measurements; they are broadly classified as stochastic and systematic uncertainty. The bais produced due to device is accounted into systematic uncertainty whereas bais due to random variables is accounted under stochastic uncertainty. The stochastic uncertainty in temperature measurement is calculated using Student t-test [75]. A total of 5 data sets of each experiment is considered to ascertain the role of ambient temperature, natural convection currents and manual interference in the experiment. The room temperature variation of $\pm$ 2 ^{0}C (as it depends on the ambient condition of a particular day) and the thermocouple accuracy of $\pm$ 2 ^{0}C are acknowledged in the overall uncertainty calculation [18]. The variation of temperature with time, for each nano-phantom selected for the study, is shown for TC200 location in fig. 5.6. The overall uncertainity is found to be $\pm$ 15 ^{0}C. The error bars shown in fig. 5.6 are at 95 % confidence interval. On the basis of the discussion mentioned in section 3.2.1 of chapter 3, the uncertainty of $\pm$15 ^{0}C in nano-phantom can be accepted for the study.

5.4 Results and discussion

5.4.1 Influence of adjuvant on cryoablation with SHN

A comparative study is carried out to find the most efficient nanoparticle in the treatment of adjuvant assisted cryospray with SHN. The liquid cryogen is sprayed on the nano and normal phantoms, keeping the rest other parameters constant. A freezing duration of 120 s and a thawing duration of 130 s are selected for the study. A spraying distance of 18 mm is kept constant throughout the experiment [155, 156]. The position of thermocouples is kept same as shown in chapter 3.

5.4.1.1 Axial Temperature Distribution

It can be seen from the curves of transient temperature (refer fig. 5.7 and fig. 5.8) that the rate of heat transfer increases as the thermal conductivity of phantoms increases. At TC200 location, the variation in the end temperatures is not quite evident between the Al_2O_3 and MgO nano-phantoms. The trends of temperature drop are also identical. Similarly, Fe_2O_3 and normal-phantom are closely following each other. An end temperature of -111 ^{0}C, -109 ^{0}C, -98 ^{0}C and -87 ^{0}C are recorded by the thermocouple at TC200 location for MgO, Al_2O_3, Fe_2O_3 and normal phantom respectively. An appreciable difference in temperature profile is obtained at TC210 location, as -89 ^{0}C, -59 ^{0}C, -45 ^{0}C and -26 ^{0}C are the end temperatures of MgO, Al_2O_3, Fe_2O_3 and normal phantom respectively. The amount of coldness decreases as the distance from the centre of the spray increases. It has been observed that the end temperature at the TC215 location is decreased from 8 ^{0}C in the case of normal phantom to -63 ^{0}C, -36 ^{0}C, -19 ^{0}C for MgO, Al_2O_3, Fe_2O_3 nano-phantoms. The freezing of gel is not observed in any of the phantoms at TC220 and TC225 locations. The thermocouples mounted 5 mm below the surface of the gel registers a similar temperature drop. It can be seen that 0.2% w/v of magnesium oxide nanaoparticles could decrease the end temperature by 27 ^{0}C, 10 ^{0}C and 19 ^{0}C at TC500, TC510 and TC515 locations respectively as compared to the normal phantom. It should be noted here that at TC515 location the temperature difference between Magnesium Oxide nano-phantom and normal-phantom is more than the temperature difference recorded at TC510 location, because at TC515 location, marginal change in temperature is recorded for normal-phantom (refer fig. 5.8c). Aluminum Oxide and Iron Oxide nano-phantoms also decrease the end temperature compared to the normal phantom in accordance to their thermal conductivity.

Table 5.1: Cooling Rate (^{0}C/min) of nano-phantom and normal-phantom for a spraying distance of (z) = 18 mm

Position of thermocouple	MgO Nano-phantom	Al_2O_3 Nano-phantom	Fe_3O_4 Nano-phantom	Normal-phantom
TC200	55	54	49	43
TC210	44	30	22	13
TC215	31	12	9	-
TC220	-	-	-	-
TC225	-	-	-	-
TC500	27	23	16	15
TC510	11	3	2	-
TC515	2	3	1	-

"-" freezing of gel is not observed

The mechanism of ice formation is responsible for the quality of necrosis. The entries of table. 5.1 clearly suggest that Intracellular ice formation (IIF) is achieved in the vicinity of spray in MgO and Al_2O_3 nano-phantoms. Iron oxide nano-phantom and normal phantom do not show such characteristics. Hence, necrosis in these phantoms might occur due to the extracellular ice formation. However, as per the study of Rubinsky [138] and accepted range of lethal temperature (-40 ^{0}C), necrosis is guaranteed upto an axial depth of 2 mm from the centre of the spray with a diameter of 10 mm in all the nano-phantoms. The changes in thermophysical properties of nano-phantoms improve the diffusion of energy within the phantom. Hence, qualitative and quantitative enhancements in necrosis are observed. On the other hand, the normal-phantom fails to provide such result.

It should be noted here that all the experiments are conducted for the same concentration of the nanoparticles. Literature suggests that the amount of cooling increases as the loading of the nanoparticles increases. However, it is also established through experimental and numerical studies that percentage increase in adjuvant is not directly proportional to the amount of cooling [132, 180]. Hence, optimum concentration of nanoparticles should be ascertained before proceeding with the clinical trials.

5.4.1.2 Radial temperature distribution

The diameters of the lethal front (temperature < -40 ^{0}C) and freezing front (temperature < 0 ^{0}C) across the surface of gel obtained from the thermal images are mentioned in table. 5.2 for the various phantoms used in the study. The images are captured at an interval

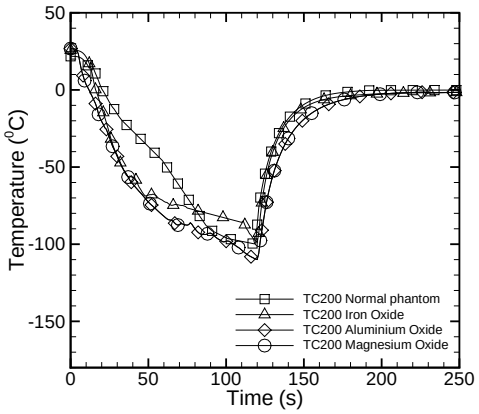

(a) 2 mm below gel surface and 0 mm away from centre of spray (TC200 location)

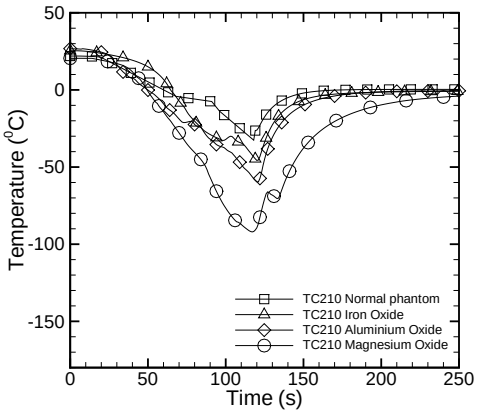

(b) 2 mm below gel surface and 10 mm away from centre of spray (TC210 location)

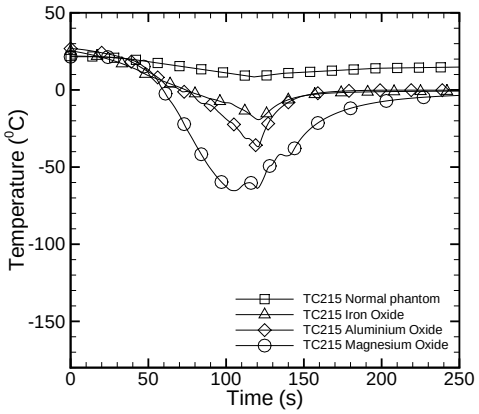

(c) 2 mm below gel surface and 15 mm away from centre of spray (TC215 location)

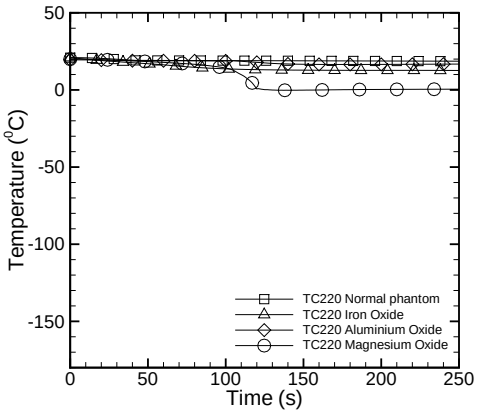

(d) 2 mm below gel surface and 20 mm away from centre of spray (TC220 location)

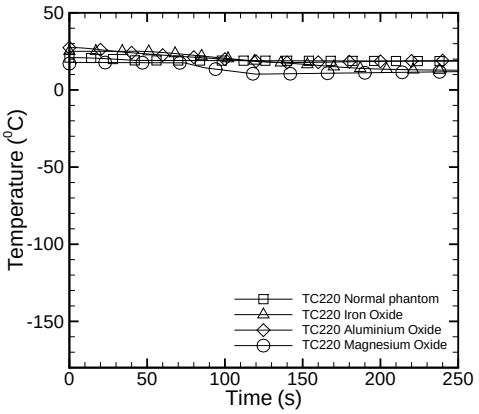

(e) 2 mm below gel surface and 25 mm away from centre of spray (TC225 location)

Figure 5.7: Transient temperature curves of thermocouples placed at 2 mm below the gel surface and at different radial locations for different phantoms

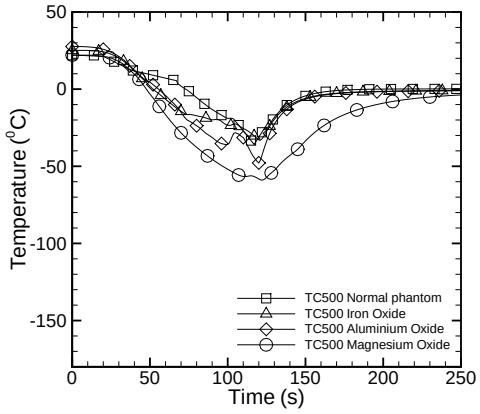

(a) 5 mm below gel surface and 0 mm away from centre of spray (TC500 location)

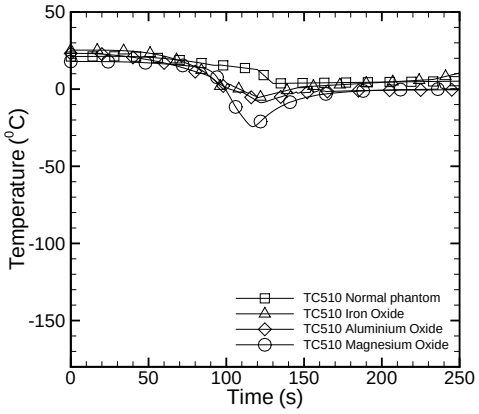

(b) 5 mm below gel surface and 10 mm away from centre of spray (TC510 location)

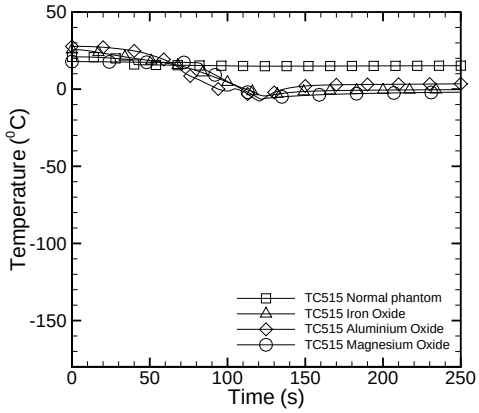

(c) 5 mm below gel surface and 15 mm away from centre of spray (TC515 location)

Figure 5.8: Transient temperature curves of thermocouples placed at 5 mm below the gel surface and at different radial locations for different phantoms

Table 5.2: Movement of lethal front and freezing front (in mm) on the gel surface with respect to time

Time (s)	MgO Nano-phantom		Al_2O_3 Nano-phantom		Fe_3O_4 Nano-phantom		Normal-phantom	
	-40^{0}C	0^{0}C	-40^{0}C	0^{0}C	-40^{0}C	0^{0}C	-40^{0}C	0^{0}C
30	18	36	17	33	14	30	6	13
60	20	38	19	35	17	34	16	24
90	25	42	22	39	21	32	18	26
120	31	48	25	45	23	42	20	30

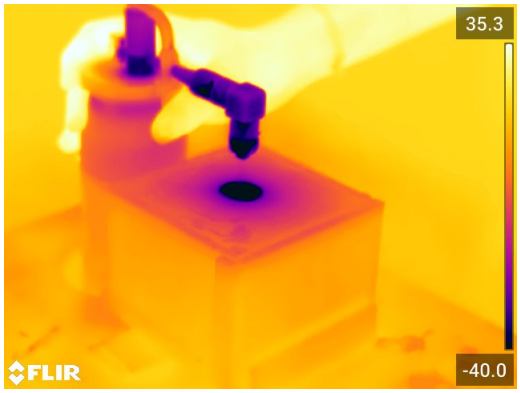

Figure 5.9: Thermal image of Al_2O_3 nano-phantom after 120 s of spray

of every 10 s during the spray of cryogen. A distinctive trend is always observed in the geometry of the skin cancer, i.e. more lateral spread on the skin as compared to the penetration depth into the skin [67]. Thus, semi-elliptic ice ball is always desired in majority of the cases. In this regard, radial temperature distribution provides the data regarding the semi-major axis of the ellipse. The thermal image of Al_2O_3 nano-phantom is shown in fig. 5.9 for the reference purpose. In the present case, lethal temperature is considered as -40 ^{0}C so that the analysis can be applicable for all types of lesion [60, 63, 139]. The entries of table. 5.2 suggest that after 120 s of spray, the diameter of lethal front of MgO nano-phantom is 24%, 34% and 55% larger than the diameter of the lethal front of Al_2O_3, Fe_3O_4 and normal phantom respectively. Whereas the diameter of freezing front of MgO nano-phantom is 7%, 14% and 60% larger than the diameter of the freezing front of Al_2O_3, Fe_3O_4 and normal phantom respectively. The presence of nanoparticles in the phantom acts as a nucleation cite for ice ball which encourages the hetrogeneous ice formation [180]. Moreover, hydrophilic nature of metallic oxide nanoparticles facilitates the nucleation of ice by decreasing the gibbs free energy [45, 102, 189]. It can be attributed as a reason for such a larger ice ball in the case of nano-phantoms.

5.4.2 Influence of adjuvant on cryoablation with MHN

It has been observed in the aforementioned study that most efficient cryoablation is obtained through MgO nanoparticles when SHN is used to spray the cryogen on nano-phantom. Thus, altogether 6 MHNs are selected to spray cryogen on MgO loaded nano-phantom with a freezing cycle of 120 s followed by a natural thawing to obtain the best MHN in terms of cryoablation . A comparative study is also carried out to demarcate the influence of adjuvants on cryoablation when the same MHNs are used to spray cryogen on nano-

Table 5.3: Difference in end temperature of nano-phantom and normal phantom [155]

Position of thermocouple	5A	5B	5C	4A	4B	4C
TC200	4	1	1	4	4	5
TC210	31	13	4	8	51	36
TC215	59	53	15	48	72	56
TC220	53	59	35	15	28	16
TC225	9	17	7	1	10	0
TC500	1	7	5	6	3	11
TC510	6	14	23	18	24	27
TC515	36	33	31	39	50	51

phantom and normal-phantom. The spraying distance is taken as 18 mm in the present study.

5.4.2.1 Axial Temperature Distribution

The temperature distribution in nano-phantom at different axial locations is shown in fig. 5.10 and fig. 5.11. At TC200 location, as the margin among the holes increases the end temperature increases. The end temperatures obtained by MHNs 5A, 5B and 5C are -158 ^{0}C, -146 ^{0}C and -144 ^{0}C whereas -157 ^{0}C, -145 ^{0}C and -128 ^{0}C are the end temperatures obtained from MHNs 4A, 4B and 4C respectively. Table 5.3 lists the difference in the end temperatures of the nano-phantom and the normal-phantom. The entries of table 5.3 suggest similar observations in normal phantom, because appreciable difference in end temperature of nano-phantom and normal-phantom is not observed. It also reflects that the role of adjuvants in cryoablation is less pronounced at TC200 location. At TC210 location, MHNs with 5 holes follow similar trend of the temperature variation with respect to time as the margin among the holes increases. However in the case of MHNs with 4 holes, 4B registers the lowest end temperature followed by 4A and 4C respectively. The end temperatures registered by MHNs 5A, 5B, 5C, 4A, 4B and 4C are -142 ^{0}C, -138 ^{0}C , -129 ^{0}C, -113 ^{0}C, -123 ^{0}C and -113 ^{0}C respectively. Moreover, at TC210 location, scenario of difference in end temperature of nano-phantom and normal-phantom is quite different from the former location (TC200). An appreciable difference in the end temperature is registered by each MHN; MHNs 5A and 4B record highest difference in their respective categories. An enhanced thermal conductivity and a reduced specific heat of nano-phantom are the reasons for such variation [26]. Apart from that, the effect of margin among the holes on cryoablation can be ascertained from the temperature readings of MHNs with 4 holes at TC210 location in nano-phantom. The MHN 4B continues to provide maximum cooling in case of MHNs with 4 holes at TC215 location whereas in the case of MHNs with 5 holes,

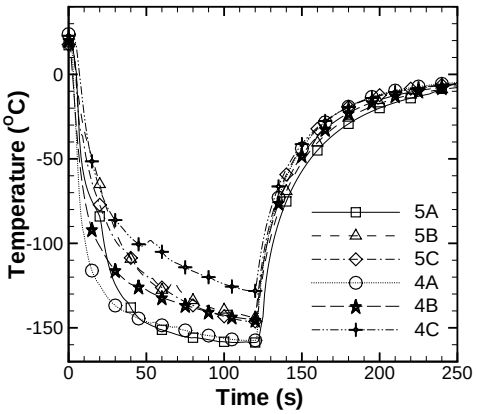

(a) 2 mm below gel surface and 0 mm away from centre of spray (TC200 location)

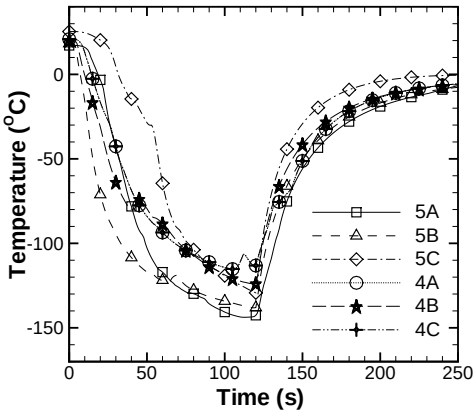

(b) 2 mm below gel surface and 10 mm away from centre of spray (TC210 location)

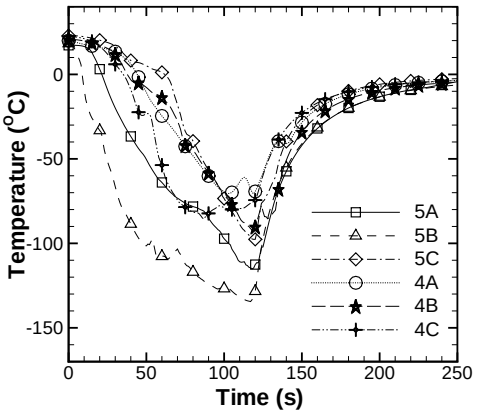

(c) 2 mm below gel surface and 15 mm away from centre of spray (TC215 location)

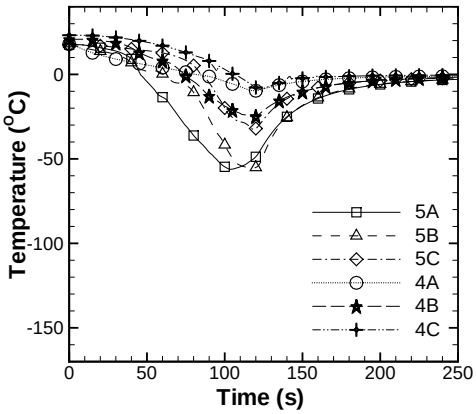

(d) 2 mm below gel surface and 20 mm away from centre of spray (TC220 location)

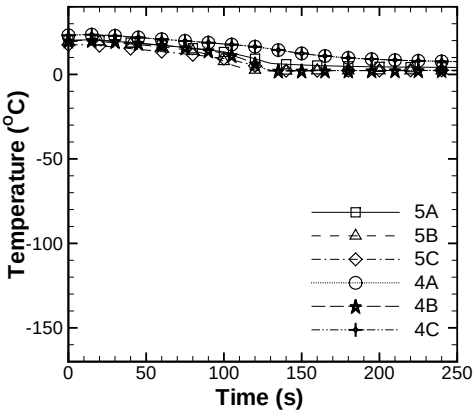

(e) 2 mm below gel surface and 25 mm away from centre of spray (TC225 location)

Figure 5.10: Transient temperature curves of thermocouples placed at 2 mm below the gel surface and at different radial locations

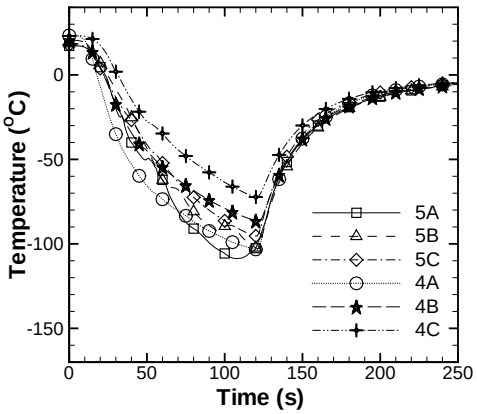

(a) 5 mm below gel surface and 0 mm away from centre of spray (TC500 location)

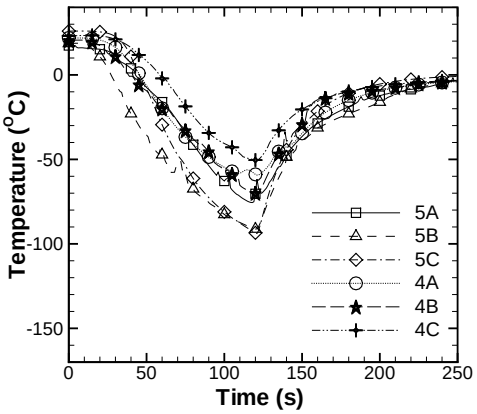

(b) 5 mm below gel surface and 10 mm away from centre of spray (TC510 location)

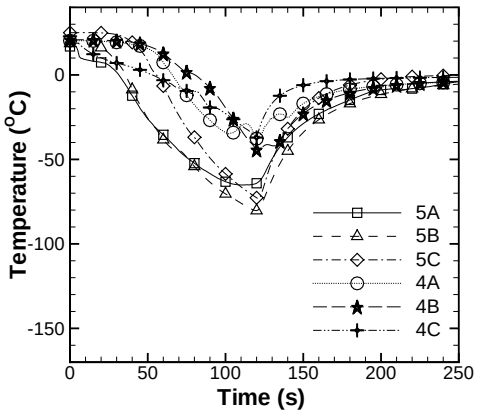

(c) 5 mm below gel surface and 15 mm away from centre of spray (TC515 location)

Figure 5.11: Transient temperature curves of thermocouples placed at 5 mm below the gel surface and at different radial locations

5B provides the lowest end temperature than MHNs 5A and 5C respectively. The trends of end temperature at TC210 and TC215 locations indicate the role of margin among the holes and the central hole in cryoablation. The effect of margin is observed near the centre of the spray (at TC210 location) in the case of MHN with 4 holes whereas in the case of MHN with 5 holes, it is observed at TC215 location. The presence of central hole can be the reason for such behavior. Due to the presence of the central hole, mass flow rate of cryogen increases and the rate of evaporation from each individual jet reduces, thus larger droplets (in terms of diameter) strike the phantom surface which causes the formation of larger spray zone on the phantom surface. Therefore, in MHNs with 5 holes, the influence of margin is obtained away from the centre of the spray than in the MHNs with 4 holes. Similarly, -48 ^{0}C, -55 ^{0}C , -32 ^{0}C, -9 ^{0}C, -24 ^{0}C and -27 ^{0}C are the end temperatures registered by MHNs 5A, 5B, 5C, 4A, 4B and 4C respectively at TC220 location. It is important to mention here that freezing is not observed at TC225 location. Moreover, it is interesting to note here that as the distance from the centre of the spray increases, the difference between the end temperatures of nano-phantom and normal-phantom increases (refer table 5.3). It reflects that adjuvant assisted approach increases cryoablation in the peripheral region of the spray zone. Similar observation is reported by Yan and liu [180]; they concluded that intentional loading of nanoparticles in tissue can lower the end temperature and increase the area of cryoablation. The thermocouples placed at 5 mm below the gel surface replicate the trends of end temperature as followed by thermocouples placed at 2 mm below the gel surface. A lower end temperature in nano-phantom is obtained at each location compared to the normal-phantom. Among the 6 MHNs selected in the study, MHNs 5B and 4B provide the most optimised result in terms of cryoablation in their respective categories.

Table 5.4 lists the cooling rate for nano-phantom and normal-phantom at the discrete locations of thermocouple. It can be interpreted through the entries of table 5.4 that the presence of adjuvants increases the zone of IIF. In case of normal-phantom, IIF is observed upto TC210 location for MHNs with 5 holes whereas in nano-phantom, IIF is observed with each nozzle. It reflects that the adjuvants assist in the rapid diffusion of coldness. Similarly, at TC215 location, IIF is not observed with any MHN in normal-phantom whereas it is observed in nano-phantom (for MHNs with 5 holes). Furthermore, cooling rate is increased at each location in the case of nano-phantom. Extracellular ice formation (EIF) is the dominant mechanism of cellular destruction when cooling rate is below 50 ^{0}C/min and considered as less lethal. So, necrosis can be assured at TC215, TC510 and TC515 locations through EIF in the nano-phantom. Thus, it can be concluded that the presence of adjuvant has increased the necrosis both quantitatively and qualitatively.

Table 5.4: Cooling rate (^{0}C/min) of nano-phantom and normal phantom [155]

Position of thermocouple	Nano-phantom						Normal-phantom					
	5A	5B	5C	4A	4B	4C	5A	5B	5C	4A	4B	4C
TC200	79	72	73	78	72	64	77	73	72	76	70	61
TC210	71	69	64	56	61	56	55	62	62	52	36	38
TC215	56	64	52	34	51	37	26	37	41	10	9	9
TC220	24	27	16	4	12	3	-	-	1	-	-	-
TC225	-	-	-	-	-	-	-	-	-	-	-	-
TC500	61	61	47	51	43	36	50	47	45	48	44	30
TC510	35	45	46	29	34	25	32	38	35	20	22	11
TC515	32	40	36	17	22	18	14	23	20	-	-	-

"-" Freezing of gel is not observed.

Table 5.5: Movement of lethal front and freezing front (in mm) on the gel surface after 120 s of spray

Multihole Nozzle	Nano-phantom		Normal-phantom	
	Lethal front	Freezing front	Lethal front	Freezing front
5A	43	78	34	50
5B	42	82	30	50
5C	41	80	32	46
4A	36	80	32	46
4B	36	74	30	45
4C	34	72	28	42

5.4.2.2 Radial temperature distribution

Table 5.5 represents the diameter of lethal front (temperature < -40 ^{0}C) and freezing front (temperature < 0 ^{0}C) formed on the surface of nano-phantom and normal-phantom. The entries of table 5.5 suggest that in the case of nano-phantom, as the margin among the holes increases, the area of necrotic zone reduces in MHNs with 5 holes. Moreover, MHNs with 4 holes follow the similar trend. It should be noted here that as the margin among the holes increases the spray zone of cryogen increases but the cooling capacity decreases which can be attributed as a reason to such variation. The cooling capacity decreases because the distance between each individual jet increases leading to more evaporation of cryogen during its flight from the nozzle exit to the phantom surface due to the entertainment of ambient air. On the basis of radial temperature distribution, MHN 5A provides the most optimised result among the 6 nozzles selected in the study and MHN 4B provides the maximum cryobalation in MHNs with 4 holes. However, on the basis of axial temperature distribution MHN 5B provides the most optimised result. The area of necrotic zone of 5A, 5B and 5C is 59 %, 96 % and 64 % larger in nano-phantom than in the normal-phantom

respectively. Similarly, the area of necrotic zone in nano-phantom is 26 %, 44 % and 30 % larger than in normal-phantom for 4A, 4B and 4C respectively. The diameter of freezing front is almost twice larger than the diameter of lethal front in nano-phanotm for each MHN whereas such trend is not observed in the normal-phantom. It reflects that the energy diffusion ability of agarose gel increases with the presence of nanoparticles.

5.5 Conclusion

The proposed study explores the possibility to enhance the scope of conventional cryospray through the introduction of adjuvant in the tissue. It can be concluded from the results that the presence of nanoparticles in phantom assists in the formation of larger ice ball. The diameter of necrotic zone on the surface of the gel in case of MgO nano-phantom is 11 mm larger than the normal-phantom. Based on the data of cooling rate, IIF is observed in closed vicinity of centre of spray in nano-phantom whereas in normal-phantom, it is absent. The proposed approach of using nanoparticles as adjuvant eliminates a major drawback associated with the use of the cryospray, i.e. current spraying technique (SHN) is applicable only to lesions of less than 15 mm in diameter. The lesions up to 30 mm in diameter with an axial depth of 2 mm can be treated effectively through the addition of MgO nanoparticles during the cryospray process. Whereas, nano-phantom with Al_2O_3 and Fe_3O_4 are suitable for lesions upto a diameter of 20 mm and 15 mm with an axial depth of 2 mm from the surface respectively.

More than 60% increment in the area of cryoablation is observed on the surface of the gel phantom when cryogen is sprayed through a MHN with 5 holes on nano-phantom than normal phantom. Intracellular ice formation is predicted upto a radius of 15 mm from the centre of the spray at an axial depth of 2 mm for MHNs with 5 holes. However, it decreased to a radius of 10 mm from the centre of the spray at an axial depth of 2 mm for MHNs with 4 holes. Among the six MHNs used in the study, MHN 5B provided the most optimised result in terms of cryoablation.